PERGAMON

International Journal of Heat and Mass Transfer 42 (1999) 3643–3657

International Journal of HEAT and MASS TRANSFER

www.elsevier.com/locate/ijhmt

Growth and collapse of a vapor bubble in a small tube

H. Yuan, H.N. Oğuz, A. Prosperetti*

Department of Mechanical Engineering, The Johns Hopkins University, Baltimore, MD 21218, USA

Received 21 October 1998; received in revised form 10 December 1998

Abstract

A model for the description of the growth and collapse of a vapor bubble in a small tube is presented and some typical results are illustrated. It is found that the maximum volume of the bubble and its lifetime depend in a complex way on the channel geometry and the initial energy distribution. However, during most of the bubble's lifetime, the internal pressure is very small and the dynamics mostly governed by the external pressure. The motivation for this work is offered by the possibility to use vapor bubbles as actuators in fluid-handling microdevices. © 1999 Elsevier Science Ltd. All rights reserved.

1. Introduction

The silicon microfabrication techniques recently developed render new technologies possible and novel regions of parameter space worthy of study. An example is the use of gas or vapor bubbles as actuators without mechanical moving parts. An intriguing possibility explored in Ref. [1] is a micropump based either on a Marangoni effect or on the suitably phased growth and collapse of bubbles generated by small heaters in liquid-filled microchannels.

The device described in Ref. [1] operates at frequencies of the order of 1 Hz in tubes with a diameter of a few micrometers. While that size range may be useful for some applications, here we are interested in tubes with a diameter of the order of a hundred micrometers that are of interest, for example, for drug delivery, on-chip chemical analysis, and others [2–5]. The exploration of vapor bubble formation in this size range is in a very early stage. A limited number of papers [6,7] deal with boiling in confined spaces and narrow gaps [8]. Models of bubbles growing in pores and pore networks are encountered in the literature on boiling in porous media [9,10], but in all these situations heat transfer to the bubble occurs from the entire solid surface rather than from a very localized heated region as in the situation of present concern. A similar comment applies to papers motivated by phase-change phenomena in micro heat pipes [11,12].

Closer to the situation investigated here is the modeling of drop ejection in ink-jet printers [13,14], and of bubble growth on microheaters [1,15,16]. In order to deal with the rather formidable difficulties of the problem, these models contain several idealizations that we try to improve upon in the present paper. We allow for the presence of more than one spatial dimension in the problem, for the momentum of the liquid, the presence of the tube wall, and several other effects. While the present model can in no way claim to be definitive, it is less idealized than others and sheds an interesting light on several of the controlling aspects of the phenomenon. For example, one of the interesting conclusions of the study is the extreme brevity of the time during which the bubble internal pressure is large. During most of the bubble life, the internal pressure is

* Corresponding author.

0017-9310/99/$ - see front matter © 1999 Elsevier Science Ltd. All rights reserved.
PII: S0017-9310(99)0027-7

Nomenclature

$a=a(t)$	bubble radius
A_n	coefficients in the expansion (7) of ϕ_T
B_n, C_n	coefficients in the expansions (8), (9) of $\phi_{l,r}$
D_n	coefficients in the expansion (10) of ϕ_B
c_{pV}	specific heat of the vapor
$\mathbf{e}_r$	unit vector in the radial direction out of the bubble
$\mathbf{e}_z$	unit vector in the direction of the tube axis
k	liquid thermal conductivity
$l_{l,r}$	lengths of the liquid columns on the left and right of the bubble
L	length of tube, see Fig. 1
$\mathscr{L}$	latent heat
$M_V(t)$	mass of vapor in the bubble
$\mathbf{n}$	unit normal directed out of the bubble
p	liquid pressure
$P_{l,r}$	pressures in the liquid reservoirs at the left and right of the tube, see Fig. 1
$P(t)$	pressure in the bubble
P_{sat}	saturation vapor pressure
r	radial coordinate in the cylindrical system, see Fig. 1
r_B	radial coordinate in the spherical coordinate system centered at the bubble center
R_T	tube radius, see Fig. 1
$\mathbf{u}$	velocity
S_B	bubble surface
t	time
$T_S(t)$	surface temperature of the bubble
T_∞	undisturbed liquid temperature
V_B	bubble volume
$\mathbf{V}_k$	velocity of the kth collocation point on the bubble surface
$V_{l,r}$	liquid velocities at the left and right ends of the tube
z	axial coordinate in the cylindrical system, see Fig. 1
$Z_B(t)$	position of the bubble center in the cylindrical coordinate system

Greek symbols

δ	parameter for grid control
ΔT	parameter characterizing the initial temperature distribution
ϵ	adjustable parameter defined in Eq. (28)
θ_B	angular coordinate in the spherical coordinate system centered at the bubble center
λ	parameter characterizing the initial temperature distribution
μ	liquid viscosity
ρ_V	vapor density
ρ_{sat}	saturation vapor density
ϕ_B	contribution of the bubble surface to the velocity potential
ϕ_l	contribution of the tube left end to the velocity potential
ϕ_r	contribution of the tube right end to the velocity potential
ϕ_T	contribution of the tube wall to the velocity potential
Φ	velocity potential
$\Phi_{\pm\infty}$	values of the potential in the reservoir far away from the tube ends
σ	surface tension coefficient

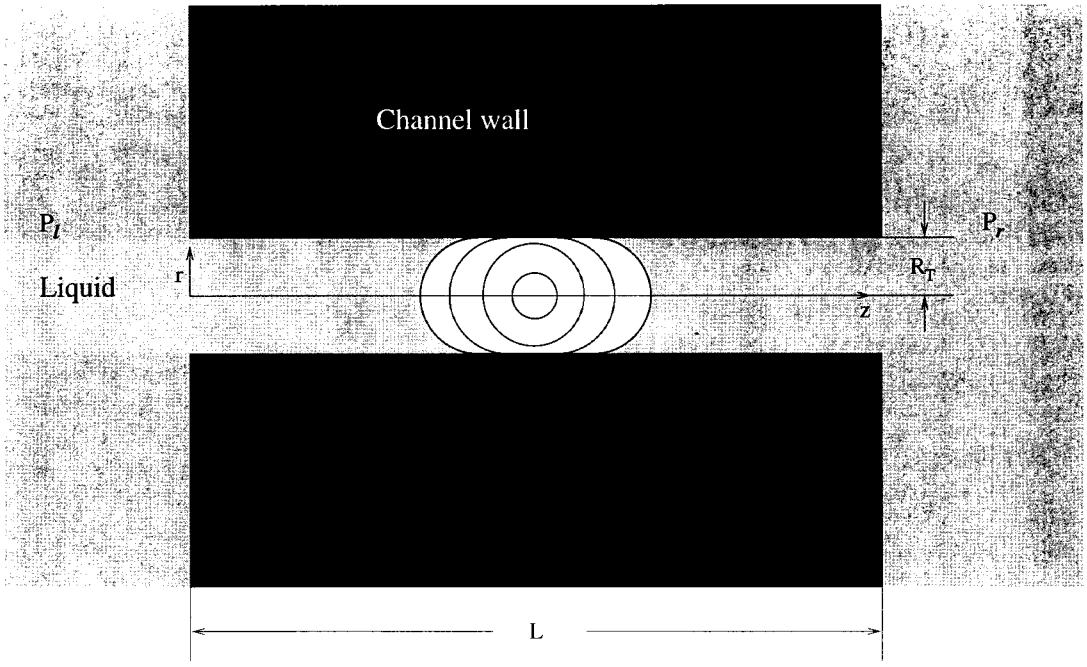

Fig. 1. Sketch of the model studied in this paper. When the bubble is sufficiently small, it is approximated as a sphere. After it has grown to nearly occlude the tube, it is approximated as a cylinder with two hemispherical caps.

negligibly small and the motion occurs therefore under the action of the external pressure alone.

2. Formulation

We assume cylindrical symmetry stipulating the bubble is generated and remains on the tube axis. We take the bubble to be a sphere from inception until its radius is nearly equal to the tube radius. Further growth is modeled by inserting a cylindrical volume between two hemispheres as shown in Fig. 1. We refer to these two stages as the *spherical* and *elongated* bubble stage, respectively. When the bubble collapses, we switch back from the elongated to the spherical model when the height of the cylindrical volume becomes zero.

In setting up our mathematical model we exploit the fact that, in order to have a repeatable and reliable bubble generation not dependent on the presence of nucleation sites, whose randomness would render the operation of the device irregular, it is necessary to rely on spontaneous nucleation. This requires high temperatures, with the consequence that the initial bubble growth is fast, with a velocity of the order of 2 m/s. For a 100 μm channel and a liquid like water we thus have a Reynolds number of the order of several hundreds. Furthermore, the phenomenon is highly transient with large accelerations, which also contribute to rendering inertia a dominant effect. Thus the early stages of the process can be treated neglecting viscous effects. The same approximation is also valid near the end of the bubble life, when most of the energy has been converted to kinetic form. These considerations suggest that viscosity is only important during the intermediate phases of the bubble lifetime, which we identify with the phase where the elongated bubble model is employed. During the spherical bubble stage, we solve numerically, by an orthogonal expansion/collocation method, the potential flow problem of a sphere expanding or collapsing inside a cylinder. When we switch to a quasi-one-dimensional model, viscous effects are included approximately. Heat transfer is accounted for in an approximate way in both regimes.

We present separate formulations for the fluid mechanics and the heat transfer aspects of the problem.

2.1. Fluid mechanics

We introduce a velocity potential Φ satisfying the Laplace equation, in terms of which the velocity $\mathbf{u}$ is given by $\mathbf{u}=\nabla\Phi$. We assume that the tube in which the bubble grows has length L, radius R_T, and connects two liquid-filled reservoirs where the pressures far away from the tube ends are $P_l(t)$, $P_r(t)$, respectively (Fig. 1).

As in Ref. [17], it is found that an appropriate form for the Bernoulli integral is

$$\frac{\partial \Phi}{\partial t} + \frac{1}{2}u^2 + \frac{p}{\rho} = \frac{P_l + P_r}{2\rho} \tag{1}$$

where p is the liquid pressure. The boundary conditions on Φ on the tube's left and right end-surfaces may be approximated by [18–20]

$$\Phi + R_T \mathbf{n} \nabla \Phi = \Phi_{\pm\infty}, \quad \text{at} \quad z = 0, L, \tag{2}$$

where the unit normal $\mathbf{n}$ is directed outside the tube volume and $\Phi_{\pm\infty}$ are the values of the potential in the reservoirs far away from the tube and given by

$$\Phi_{\pm\infty} = \pm\frac{1}{2}\int_0^t \frac{P_l - P_r}{\rho}\, dt. \tag{3}$$

On the tube wall the normal velocity vanishes

$$\left.\frac{\partial \Phi}{\partial r}\right|_{r=R_T} = 0. \tag{4}$$

In the following we need to distinguish the stages of the process during which the bubble is assumed to be spherical, from that in which the bubble is elongated.

2.1.1. Spherical bubble

We assume the pressure $P(t)$ inside the bubble to be spatially uniform and dependent on time only. Upon imposing that the difference between the bubble internal and external pressure be balanced by the effect of surface tension, the Bernoulli integral evaluated at the bubble surface gives

$$\frac{\partial \Phi}{\partial t} + \frac{1}{2}u^2 + \frac{P - \sigma\mathscr{C}}{\rho} = \frac{P_l + P_r}{2\rho}, \tag{5}$$

where σ is the surface tension coefficient and $\mathscr{C}$ the curvature.

The boundary of the computational domain consists of the bubble surface, the tube surface, and two circles at the left and right ends of the tube separating the tube volume from the reservoirs. We express the velocity potential as a superposition of several terms as follows [17]:

$$\Phi = \phi_B + \phi_T + \phi_l + \phi_r. \tag{6}$$

Each term is a solution of the Laplace equation built in such a way that, on each of the surfaces into which the total boundary of the problem can be decomposed (i.e., the bubble, the lateral surface of the tube, and the left and right circles), it reduces to a complete set of eigenfunctions. As will be shown below, in this way a unique solution of the problem can be found. Thus we take

$$\phi_T = \sum_{n=1}^{\infty} A_n I_0\left(\frac{n\pi r}{L}\right) \sin\frac{n\pi z}{L}, \tag{7}$$

where I_0 is a modified Bessel function and r, z are (global) cylindrical coordinates with origin at the center of the left end-surface of the tube and axis coincident with that of the tube (Fig. 1). By construction ϕ_T vanishes at the left and right end-surfaces of the tube.

In (6), the term ϕ_l corresponding to the contribution of the left end-surface is written as

$$\begin{aligned}\phi_l = {} & B_0(L + R_T - z) \\ & + \sum_{n=1}^{\infty} B_n J_0\left(j_n \frac{r}{R_T}\right)\left[\sinh\left(j_n \frac{z}{R_T}\right)\right. \\ & \left. - \frac{\tanh(j_n L/R_T) + j_n}{1 + j_n \tanh(j_n L/R_T)} \cosh\left(j_n \frac{z}{R_T}\right)\right],\end{aligned} \tag{8}$$

where J_0 is the Bessel function of order 0 and the j_ns are the zeros of J_1. This expression satisfies the boundary condition (2) on the circle at the right end of the tube and the condition (4) on the tube wall. The contribution of the right end-surface, satisfying analogous boundary conditions, is similar:

$$\begin{aligned}\phi_r = {} & C_0(z + R_T) \\ & + \sum_{n=1}^{\infty} C_n J_0\left(j_n \frac{r}{R_T}\right)\left[\sinh\left(j_n \frac{L - z}{R_T}\right)\right. \\ & \left. - \frac{\tanh(j_n L/R_T) + j_n}{1 + j_n \tanh(j_n L/R_T)} \cosh\left(j_n \frac{L - z}{R_T}\right)\right].\end{aligned} \tag{9}$$

For the contribution ϕ_B of the bubble we write

$$\phi_B = \sum_{n=0}^{\infty} D_n \left(\frac{a}{r_B}\right)^{n+1} P_n(\cos\,\theta_B), \tag{10}$$

where $a = a(t)$ is the bubble radius, the P_ns are Legendre polynomials, and we have introduced a local spherical coordinate system (r_B, θ_B), with the origin at the center of the bubble and the polar axis coincident with the positive z-axis of the global cylindrical system. Local and global coordinates are related by

$$r_B = \sqrt{(z - Z_B)^2 + r^2}, \quad \cos\,\theta_B = \frac{z - Z_B}{r_B}, \tag{11}$$

where $Z_B(t)$ is the position of the bubble center in the cylindrical coordinate system. The inverse relations are

$$z = Z_B + r\,\cos\,\theta_B, \quad r = r_B\,\sin\,\theta_B. \tag{12}$$

In the global coordinate system, the surface of the bubble is defined by $z = \xi(s)$, $r = \eta(s)$, where s is the arc length along the surface of the bubble in the meridian plane.

The rationale for the form (6) of Φ can now be explained as follows. Consider, for example, the

boundary condition (4) of vanishing normal velocity at the tube surface. Since $\phi_{l,r}$ already satisfy this condition by construction, we find, for $r=R_T$,

$$\sum_{n=1}^{\infty}\frac{n\pi}{L}A_nI_1\left(\frac{n\pi R_T}{L}\right)\sin\frac{n\pi z}{L}=-\left.\frac{\partial\phi_B}{\partial r}\right|_{r=R_T}. \tag{13}$$

Upon taking a scalar product with $\sin(n\pi z/L)$, we have

$$A_n=-\left[\frac{n\pi}{L}I_1\left(\frac{n\pi R_T}{L}\right)\right]^{-1}\frac{2}{L}\int_0^L \mathrm{d}_z \sin\frac{n\pi z}{L}\left.\frac{\partial\phi_B}{\partial r}\right|_{r=R_T}, \tag{14}$$

which, from (10), expresses the coefficients $\{A_n\}$ in terms of the $\{D_n\}$. In a similar fashion, upon substituting Φ into the boundary condition (2) at the left of the tube, we have

$$B_0(L+2R_T)-\sum_{n=1}^{\infty}B_nJ_0\times\left(j_n\frac{r}{R_T}\right)\frac{2j_n+(j_n^2+1)\tanh(j_nL/R_T)}{1+j_n\tanh(j_nL/R_T)} =\Phi_{-\infty}-\phi_B|_{z=0}+R_T\left.\frac{\partial}{\partial z}(\phi_T+\phi_B)\right|_{z=0}. \tag{15}$$

From this equation, the coefficients $\{B_n\}$ can be related to the others by using the completeness and orthogonality of the $J_0(j_nr/R_T)$. The analogous relation at $z=L$ is

$$C_0(L+2R_T)-\sum_{n=1}^{\infty}C_nJ_0\left(j_n\frac{r}{R_T}\right)\frac{(j_n^2+1)\tanh(j_nL/R_T)+2j_n}{1+j_n\tanh(j_nL/R_T)} =\Phi_{\infty}-\phi_B|_{z=L}-R_T\left.\frac{\partial}{\partial z}(\phi_T+\phi_B)\right|_{z=L}. \tag{16}$$

The previous relations show how the solution that we find is unique in spite of the apparent redundancy of the decomposition (6) of the potential. The point is that the sets of coefficients of each expansion can be related to each other by well-defined mathematical operations due to the key property that each term, when restricted to the corresponding surface, consists of the superposition of a complete set of functions.

2.1.2. Elongated bubble

When the bubble nearly fills the cross section and starts growing along the tube axis, we switch to a simpler fluid mechanical model in which the two liquid columns filling the channel on the left and right sides of the bubble move as rigid bodies with velocities V_l and V_r respectively.

The Bernoulli integral on the circle at the right end of the tube is

$$\frac{\partial\Phi}{\partial t}+\frac{1}{2}V_r^2+\frac{p_r}{\rho}=\frac{\partial\Phi_{\infty}}{\partial t}+\frac{P_r}{\rho}, \tag{17}$$

where V_r is the velocity of the liquid exiting the tube. The time derivative of the condition (2)

$$\frac{\partial\Phi}{\partial t}+R_T\frac{\mathrm{d}V_r}{\mathrm{d}t}+\frac{p_r}{\rho}=\frac{\partial\Phi_{\infty}}{\partial t} \tag{18}$$

can be used to eliminate $\partial\Phi/\partial t$ to find the pressure on the circle at the end of the tube:

$$\frac{p_r}{\rho}=\frac{P_r}{\rho}+R_T\frac{\mathrm{d}V_r}{\mathrm{d}t}-\frac{1}{2}V_r^2. \tag{19}$$

With this result, the equation of motion for the right liquid column becomes

$$\pi R_T^2\rho\frac{\mathrm{d}}{\mathrm{d}t}[V_r(l_r+R_T)]=\left(P-P_r-\frac{2\sigma}{a}+\frac{1}{2}\rho V_r^2\right)\pi R_T^2-8\pi l_r\mu V_r \tag{20}$$

where l_r is the length of the liquid column on the right of the bubble and μ is the liquid viscosity; the last term is an approximation to viscous losses in the tube built on the assumption of fully developed Poiseuille flow [18,21]. Similarly, for the liquid column on the left of the bubble, we have

$$\pi R_T^2\rho\frac{\mathrm{d}}{\mathrm{d}t}[V_l(l_l+R_T)]=\left(P_l-P+\frac{2\sigma}{a}+\frac{1}{2}\rho V_l^2\right)\pi R_T^2-8\pi l_l\mu V_l. \tag{21}$$

The initial value for $l_{l,r}$ is determined by calculating the volume of liquid in the tube on the left and right of the bubble at the time at which the dynamic model is switched, and dividing by πR_T^2.

In view of the assumed geometry of the problem (see Fig. 1), the two velocities are connected by the obvious relation

$$\pi R_T^2(V_r-V_l)=\frac{\mathrm{d}V_B}{\mathrm{d}t}, \tag{22}$$

where V_B is the bubble volume.

2.2. Heat transfer

We assume that the bubble surface is at a spatially uniform temperature $T_S(t)$, and that thermodynamic equilibrium conditions prevail so that $P=P_{sat}(T_S)$,

$\rho_V = \rho_{sat}(T_S)$ where ρ_V is the vapor density and the functions P_{sat}, ρ_{sat} are defined by the thermodynamic relations expressing saturated vapor–liquid equilibrium. An energy balance at the bubble surface gives [22]

$$\mathscr{L}\frac{dM_V}{dt} - M_V\left(\frac{\mathscr{L}}{T_S} - c_{pV}\right)\frac{dT_S}{dt} = -\int_{S_B} k\mathbf{n}\nabla T \, dS_B, \tag{23}$$

where $\mathscr{L}$ is the latent heat, $M_V(t)$ the mass of vapor in the bubble, c_{pV} the specific heat of the vapor, S_B the bubble surface, k the liquid thermal conductivity, and $\mathbf{n}$ the unit normal directed out of the bubble. From this equation one can obtain an expression for dT_S/dt from which T_S is found upon integration.

As before, we distinguish between the two stages in the bubble evolution.

2.2.1. Spherical bubble

Heat transfer is most intense during the initial growth of the bubble. During this stage the motion is rapid and the stretching imposed by the geometry has the effect of thinning the thermal boundary layer around the bubble surface. Hence we approximate the process by assuming that both conduction and convection are only significant in the radial direction. During this phase the energy equation in the liquid is therefore approximated as

$$\frac{\partial T}{\partial t} + \frac{a^2}{r_B^2}\dot{a}\frac{\partial T}{\partial r_B} = \frac{D}{r_B^2}\left(r_B^2\frac{\partial T}{\partial r_B}\right), \tag{24}$$

subject to

$$T(r_B = a(t),t) = T_S(t), \quad T \to T_\infty \quad \text{as} \quad r_B \to \infty, \tag{25}$$

where T_∞ is the liquid temperature far away from the bubble.

To start the problem we assume a temperature distribution in the liquid surrounding the bubble given by

$$T(r,0) - T_\infty = \Delta T \exp\left[-\frac{r - a(0)}{\lambda}\right], \tag{26}$$

where ΔT and λ are prescribed.

2.2.2. Elongated bubble

During this phase of the bubble life we use an approximation that can be viewed as a low-order collocation procedure. We write a convection equation similar to (24) for the two points of the bubble surface on the tube axis. Since these points are moving with the velocities $V_{l,r}$ of the liquid column to which they belong, we have

$$\frac{\partial T}{\partial t} + V_{l,r}\frac{\partial T}{\partial r_B} = D\left(\frac{\partial^2 T}{\partial r_B^2} + \frac{2}{R_T}\frac{\partial T}{\partial r_B}\right), \tag{27}$$

with the common boundary condition $T = T_S$ at the bubble surface.

The other 'collocation point' (or, more accurately, ring) is placed on the mid-plane of the cylindrical portion of the bubble surface. When the bubble has grown to occupy most of the tube cross section, the thin layer of liquid separating it from the tube wall is essentially stagnant (and it would, of course, be exactly stagnant at the plane of symmetry). Thus, during this stage, we simply solve two one-dimensional conduction equations, one in the liquid and one in the tube wall, coupled by the usual continuity conditions of temperature and heat flux at the solid–liquid interface. At the bubble surface we again impose $T = T_S$.

A difficulty arises, however, in switching between the two models during the growth phase because, if the bubble is exposed abruptly to the cold wall when the liquid gap has thinned sufficiently, intense condensation takes place. To avoid this unphysical behavior, it is necessary to 'preheat' the wall. This objective is accomplished by taking the temperature distribution calculated from (24) during the spherical stage, deducing from it the liquid temperature at a distance equal to the distance of the bubble surface from the wall, and using this temperature as boundary condition for the one-dimensional conduction equation in the wall.

This procedure is approximate, and it becomes gradually worse as the bubble surface gets closer to the wall since it ignores the effect of the wall on convection. Therefore, when

$$T_w - T_\infty = \epsilon(T_S - T_\infty), \tag{28}$$

with ϵ of the order of a few percent, we switch to a form of the energy equation incorporating a linear velocity field between the bubble 'equator' and the wall:

$$\frac{\partial T}{\partial t} + \frac{R_T - r}{R_T - a}\dot{a}\frac{\partial T}{\partial r} = D\left(\frac{\partial^2 T}{\partial r^2} + \frac{1}{r}\frac{\partial T}{\partial r}\right). \tag{29}$$

The assumption of a linear velocity distribution is motivated by the structure of the stagnation-point flow [23], that can be taken to approximate the situation given the relative narrowness of the liquid gap in this stage of the bubble motion. Eq. (29) is coupled with the one-dimensional conduction equation in the wall as before. In view of the brevity of the process, in these calculations we take the wall to be infinitely extended normally to the channel surface.

When the assumption of spherical symmetry is abandoned in the heat transfer model, the heat fluxes calculated at the 'poles' of the bubble (on the tube axis) and around its 'equator' will in general be different. In

these conditions, in order to approximate the surface integral (23), we assume a linear interpolation for the heat flux along the curved surface of the bubble. The heat flux along the cylindrical portion of the bubble surface is assumed to be spatially uniform.

3. Solution procedure

The mathematical formulation of the previous section is solved numerically by marching forward in time. Since, given the complexity of the model, the sequence of the calculation is not entirely straightforward, it is appropriate to describe it here in some detail. Again we distinguish between the spherical and elongated bubble stages.

3.1. Spherical bubble

Suppose that the bubble radius, radial velocity, axial position, axial velocity, and all the coefficients in the expansions are known at time t. To advance to time $t+\Delta t$ we proceed as follows. We select N equispaced points on the bubble surface and use the Bernoulli integral (5) to write the convective derivative of the potential at each one of these points. Thus, for the generic point k, we have

$$\left(\frac{D\Phi}{Dt}\right)_k \equiv \left(\frac{\partial\Phi}{\partial t}\right)_k + \mathbf{V}_k(\nabla\Phi)_k = \left(\mathbf{V}_k - \frac{1}{2}\mathbf{u}_k\right)\mathbf{u}_k + \frac{P_\mathrm{l} - P_\mathrm{r} - 2P + 2\sigma\mathscr{C}}{2\rho}, \quad (30)$$

where $\mathbf{V}_k$ is the velocity of the kth point. Since only radial and translational motion of the bubble is allowed, we have

$$\mathbf{V}_k = \dot{a}\mathbf{e}_\mathrm{r} + \dot{Z}_\mathrm{B}\mathbf{e}_z, \quad (31)$$

with $\mathbf{e}_\mathrm{r}$ a unit vector in the radial direction out of the bubble center and $\mathbf{e}_z$ a unit vector in the direction of the tube axis. With this result, we can advance the value of Φ at the N points on the bubble surface by the one-step forward Euler method:

$$\Phi(\mathbf{x}_k, t+\Delta t) = \Phi(\mathbf{x}_k, t) + \Delta t\left(\frac{D\Phi}{Dt}\right)_k. \quad (32)$$

Once Φ has been determined at the N points from this formula, from (6) we can write, on the bubble surface

$$\phi_\mathrm{B} + \phi_\mathrm{T} = \Phi - \phi_\mathrm{l} - \phi_\mathrm{r}. \quad (33)$$

The coefficients $\{A_n\}$ of ϕ_T can be expressed in terms of the $\{D_n\}$ of ϕ_B from (14), and this equation can then be solved for the $\{D_n\}$ by taking suitable scalar products (evaluated by the trapezoidal rule at the N surface points). Notice that ϕ_l and ϕ_r have not been updated yet. To achieve full consistency, this equation must be used iteratively. At the first step the previous values of ϕ_l and ϕ_r are used in the right-hand side, then these quantities are updated using (15) and (16), and the procedure is repeated until convergence. This iterative procedure would work also if ϕ_T were put in the right-hand side and treated in the same way, but only as long as the bubble is smaller than about half the tube diameter. For larger bubbles, the contribution of ϕ_T to the total potential is too large for the iterations to converge. If the bubble was very close to one of the two ends of the channel, one might expect a similar convergence difficulty and either ϕ_l or ϕ_r should be kept in the left-hand side of the equation. This difficulty, however, has not been encountered in the present simulations.

With the velocity potential at $t+\Delta t$ determined in this way, one needs to find the new radial and translational velocities of the bubble. For this purpose, we form the quantity $\mathbf{e}_\mathrm{r}\nabla\Phi$ (i.e., we take the derivative of the expression (6) for the potential with respect to the distance from the bubble center) and take a scalar product with P_0, thus obtaining $\dot{a}$, and P_1, which gives Z_B. We use the same N points on the bubble surface used before to calculate the integrals by the trapezoidal rule. The analogous scalar products with the higher-order polynomials would account for the deformation of the bubble but are disregarded in this study. With the knowledge of $\dot{a}$ and Z_B, the new bubble radius and position are calculated from the one-step forward Euler formula.

The last step is the calculation of the new pressure inside the bubble, which will be used in the Bernoulli integral to advance to the next time level. This step requires solving the energy equations. For the spherical energy equation (24) we introduce the new coordinate

$$x = \frac{\delta}{\delta + r - a(t)}, \quad (34)$$

where δ is a grid control parameter of the order of the length scale of the initial heated liquid layer (we use $\delta=\lambda$ here). The equation written in terms of x is then discretized on an equispaced grid (which, of course, is not equispaced in the original variable r) and solved subject to the boundary condition (23). The conduction equation in the wall and the other energy equation in the liquid, equation (29), are also solved by finite differences, the latter one after the variable transformation $y=(R_\mathrm{T}-r)/(R_\mathrm{T}-a)$.

After using the results of the energy equations to calculate the heat flux at the bubble surface and effecting the integral in (23), we have a value for $\mathrm{d}T_\mathrm{S}/\mathrm{d}t$, which can be used to advance the surface temperature

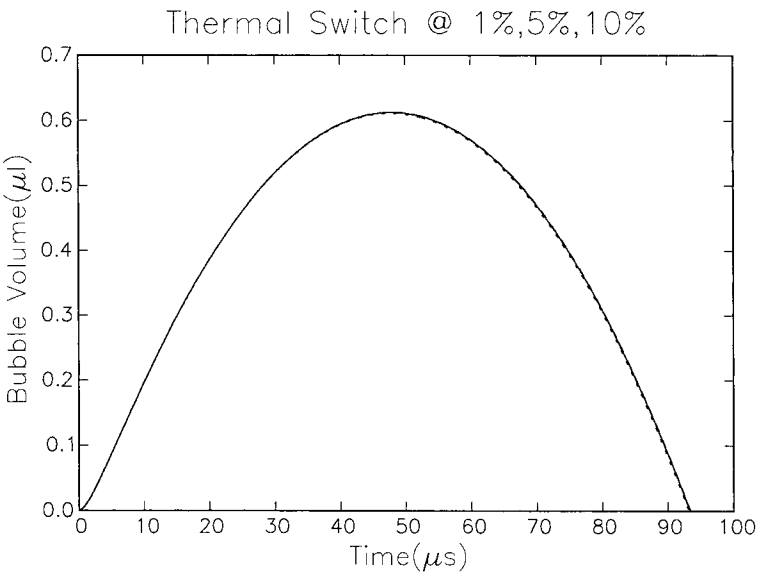

Fig. 2. Bubble volume as a function of time. Channel length and radius are 5 mm and 50 μm respectively, with $L/R_T = 100$. The initial bubble radius is 5 μm, so that $R_T/a(0) = 10$. The initial temperature distribution is given by Eq. (26) with $\Delta T = 250$ K, $T_\infty = 300$ K, $\lambda = 5$ μm. The liquid is water. In this figure the results corresponding to a switching between the spherical and elongated bubble models corresponding to values of 1%, 5%, and 10% of the parameter ϵ defined in Eq. (28) are superposed. The maximum length achieved by the bubble is about 10% of the tube length.

by the one-step Euler method, after which the new pressure and density in the bubble are found from the saturation relations.

The switching from the spherical to the elongated bubble model for the thermal treatment of the problem is gradual, as described in subsection 2.2.2. For the fluid dynamics of the problem, one can proceed more abruptly without adversely affecting the results of the simulation. When the bubble radius is predicted to be within 1% of the tube radius, we switch to the elongated bubble model of subsection 2.1.2. The mathematical structure of this model is much simpler as the bubble motion is only described in terms of ordinary differential equations in time that are solved again by the one-step Euler method.

While switching for the fluid dynamic model can be done abruptly, some care must be exerted to avoid jumps in the velocities. In going from the spherical to the elongated model, the equivalent liquid column lengths l_l, l_r are determined by conserving the mass of the liquid. The initial value of the velocities $V_{l,r}$ is determined by writing the corresponding mass balances

$$\pi R_T^2(V_l + \dot{Z}_B) = \frac{1}{2}\dot{V}_B \tag{35}$$

$$\pi R_T^2(V_r - \dot{Z}_B) = \frac{1}{2}\dot{V}_B. \tag{36}$$

These expressions assume that the bubble obstructs the tube so that, in its frame of reference, half of the liquid flows into the right half of the tube and half into the left half.

3.2. Elongated bubble

The elongated bubble model consists of the dynamical equations (20–22) and the one-dimensional conduction equations in the thin liquid film and in the adjacent solid. The energy equations are solved by finite differences. The solution of the conduction–convection Eq. (27) along the tube axis is also effected by finite differences after a coordinate transformation moving with the bubble wall, which transforms the equation to a purely conduction form due to the assumption of one-dimensional flow during this phase.

When the bubble collapses, in switching from the elongated model to the spherical model, we use these same equations to find $\dot{a}$ and $\dot{Z}_B$. However, we also have to initialize the value of the potential. For this purpose, we calculate the radial derivatives of the potential, take scalar products with P_0 and P_1, and equate the results to $\dot{R}$ and $\dot{}_B$. This procedure deter-

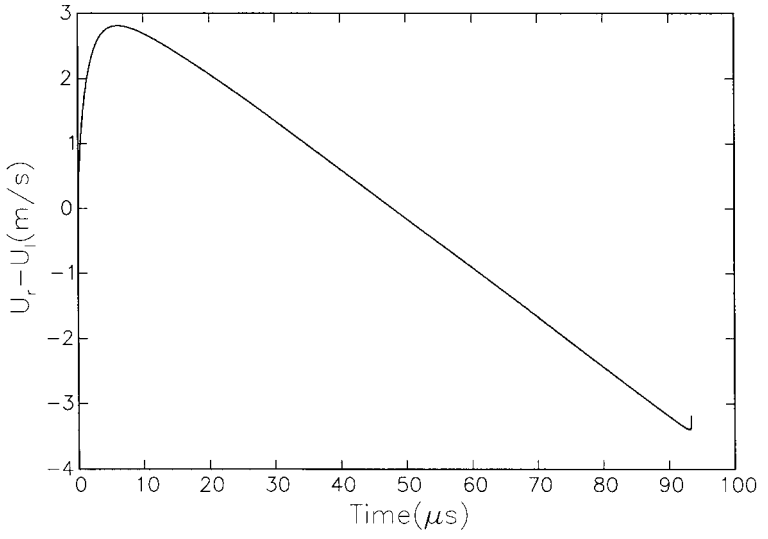

Fig. 3. Effective bubble growth velocity $\dot{V}_B/\pi R_T^2$ vs time for the case of the previous figure. Note the long linear part of the curve corresponding to essentially constant acceleration. The quantity plotted is also equal to the difference between the liquid velocities at the two ends of the tube.

mines Φ up to a function of time that is fixed by matching with the values of $\Phi_{\pm\infty}$ that are calculated all through the process from (3).

For the thermal problem the switching is done following in reverse order the steps outlined before. Firstly, Eq. (29) is used for the heat transfer around the bubble 'equator'. When the bubble wall temperature satisfies (28), we return to the fully spherical model. This stage of the bubble life is mostly governed by inertia forces and the effects of the precise criterion for the switching of the thermal model have negligible effects.

4. Results

In spite of its approximate nature, the model described in the previous sections is useful to illustrate the trends of the system behavior with changes in the many parameters that it involves. We shall do this by

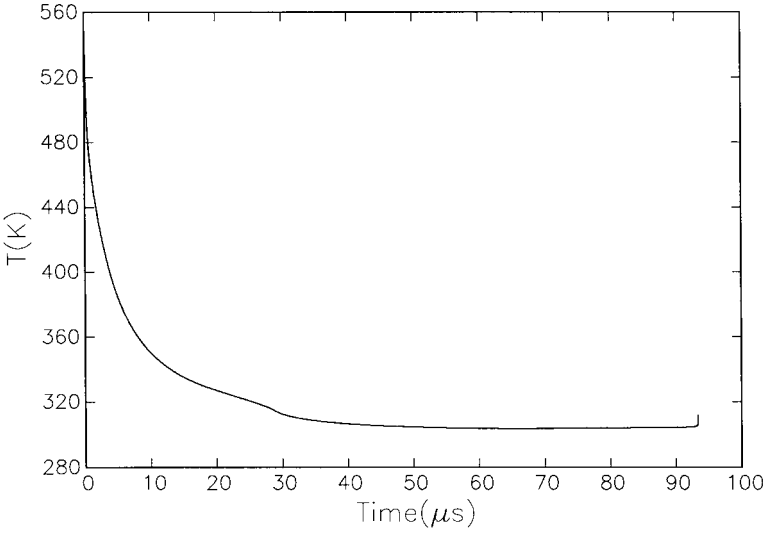

Fig. 4. Bubble internal pressure as a function of time for the case of Figs. 2 and 3.

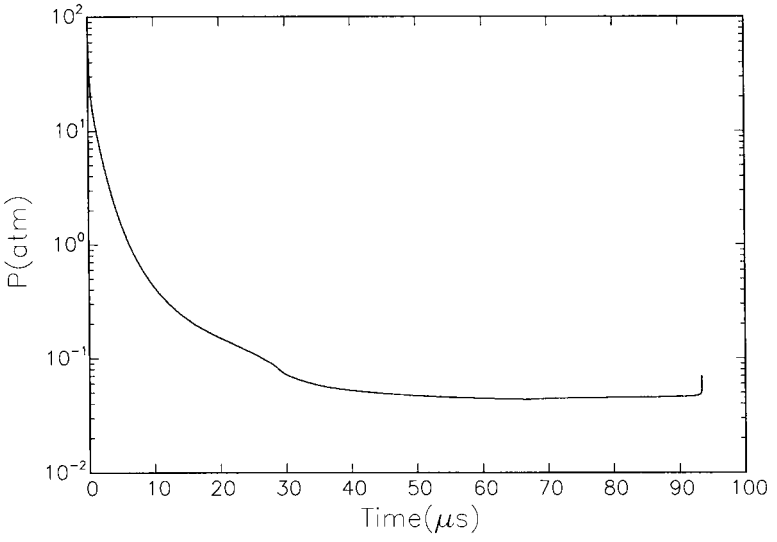

Fig. 5. Bubble surface temperature as a function of time for the case of Figs. 2–4. The increased cooling rate between 20 and 30 μs is due to the exposure to the cold wall.

comparison with a reference situation that will be described in detail first. We assume that the pressure in the two reservoirs at the ends of the tube is atmospheric, the tube length is $L=5$ mm, the tube radius $R_T=50$ μm, so that $L/R_T=100$. The liquid is water. The initial temperature distribution in the liquid is given by (26) with $\Delta T=250$ K, $T_\infty=300$ K, $\lambda=5$ μm. The initial bubble radius is taken to be $a(0)=5$ μm, so that $R_T/a(0)=10$. In making this choice we envisage an experimental situation in which the liquid is preheated by energizing the heater prior to the generation of a vapor nucleus, which is induced by a short excursion of the heater temperature above the homogeneous nucleation temperature of the liquid. When this is done, the heater becomes covered with a very thin vapor film, which can be taken to be the initial bubble

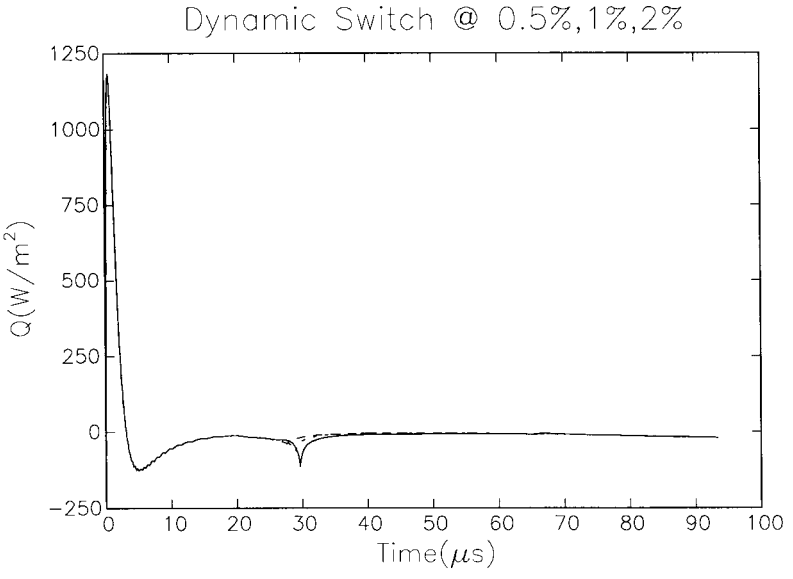

Fig. 6. Net heat flow rate into the bubble for the case of Figs. 2–5 as a function of time. The three curves (barely distinguishable from each other only around 30 μs) correspond to a switching from the spherical to the elongated bubble model when the liquid film has thinned to 0.5, 1 and 2% of the tube radius.

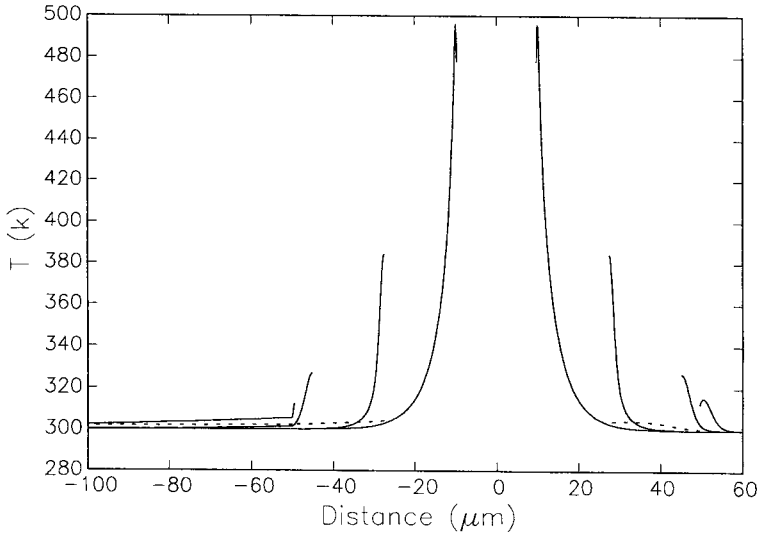

Fig. 7. Temperature distributions near the bubble of Figs. 2–6 at 0.5, 5, 20, and 30 μs, in descending order. The lines in the right half of this figure show the temperature distribution along the tube axis as functions of distance from the bubble center. The lines in the left half of the figure are the temperature distributions along the bubble equator and into the solid, that occupies the region to the left of -50 μm. The dotted lines are the temperature distributions at 90 μs, i.e. near the end of the collapse. All the lines begin at the instantaneous position of the bubble surface.

[14]. Hence, the parameter $a(0)$ essentially characterizes the heater size and the parameter λ the duration of the pre-heating phase. The use of temperatures much above the boiling point is motivated by the need to rely on homogeneous (or nearly-homogeneous) nucleation for repeatability of the process, as explained before.

Fig. 2 shows the volume of the bubble as a function of time. The curve is very regular and almost symmetric about the maximum, where the bubble length is about 10% of the total channel length. This figure actually shows three superposed lines corresponding to three values of the parameter ϵ defined in (28) which determines the point at which a switching between different thermal models is effected, $\epsilon = 1$, 5 and 10%. It is clear that the precise time at which the switching is effected has a negligible effect on the computed results. We looked at the sensitivity to the switching between the dynamic spherical and elongated bubble models (see the beginning of section 2) by effecting the transition when the spherical bubble radius was 99.5, 99 and 98% of the tube radius finding a negligible effect on the time dependence of the volume.

Fig. 3 shows $\dot{v}_B/\pi R_T^2$ vs time, i.e. the relative velocity between the two bubble surface points on the tube axis. Other than for brief instants at the beginning of the growth and at the end of the collapse, the slope of the line is very nearly constant, which indicates a motion under the action of a constant force. The explanation for this behavior is given in Fig. 4 which shows the bubble internal pressure vs time. It is seen that after about 20 μs the internal pressure becomes negligible with respect to the ambient, so that the motion is governed by the external pressure. The bubble surface temperature associated with the pressure in Fig. 4 is shown in Fig. 5. In the first 10 μs the rapid cooling (at a rate of the order of 20×10^6 K/s!) of the bubble surface is due to the expansion and rapid evaporation. The cooling process beginning between 20 and 30 μs is due to the exposure to the cold wall. Further insight into the thermal aspects of the phenomenon is provided by Fig. 6, where the heat flow rate into the bubble is plotted as a function of time. In the very first instants, according to the temperature distribution (26), the heat flows away from the bubble. This phase is, however, extremely short-lived, and the heat flow rate becomes positive and large already within the first 0.05 μs. This second phase of large heat flow into the bubble is also very short. Due to the strong cooling effects of expansion and evaporation, the heat flow reverses sign already after about 3 μs, after which it remains slightly negative (signifying a heat loss by the bubble) due to vapor condensation on the cold bubble surface. The dip around 30 μs is due to the thinning of the liquid film separating the bubble from the wall, as is clear from the three different lines apparent in this region, which correspond to stopping the thinning of the film at 0.5, 1 and 2% of the tube radius. This is the only prediction of the model that we have found to be detectably

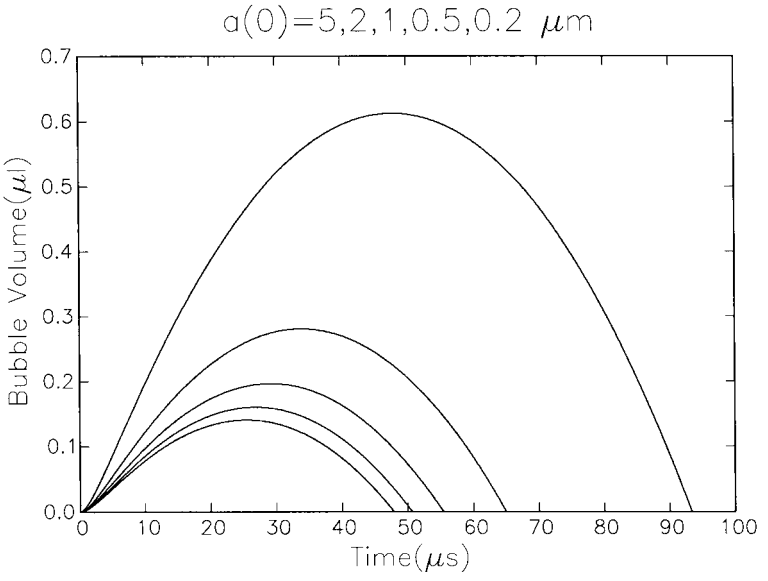

Fig. 8. Bubble volume vs time for initial bubble radii $a(0)=0.2$, 0.5, 1, 2, and 5 μm (in ascending order) for a given fixed amount of initial liquid thermal energy. All other conditions as in Fig. 2.

sensitive to the switching between the spherical and elongated bubble models. However its impact on the overall behavior, and in particular on the total heat transfer, is quite negligible. The heat flow rate reaches practically zero as the bubble surface temperature reaches the ambient value, and then becomes slightly negative as the bubble volume decreases and vapor condenses. It is also interesting to look at the temperature distribution for points on the axis of the tube and along the equator of the bubble and into the solid wall (Fig. 7). The solid lines in the right half of this figure show the temperature distribution in the liquid during the bubble growth at times 0.5, 5, 20, and 30 μs as functions of distance from the bubble center. The lines

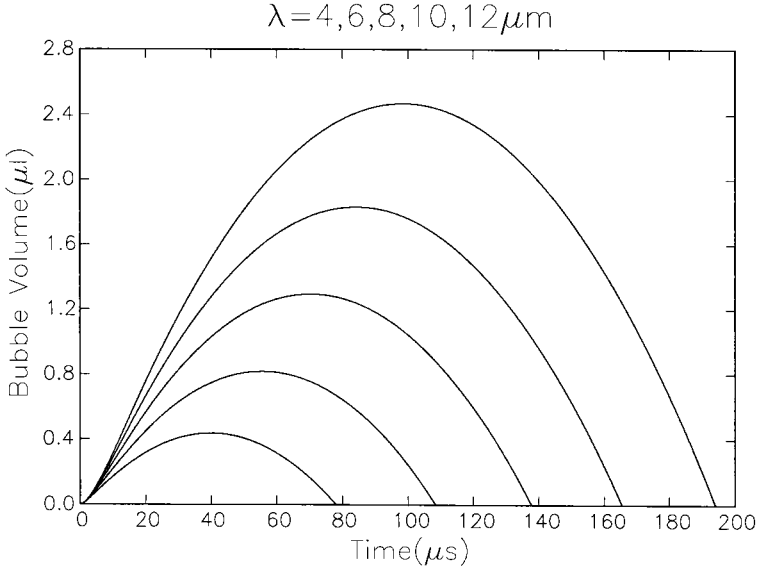

Fig. 9. Bubble volume vs time for different initial liquid temperature distributions Eq. (26) with $\lambda=4$, 6, 8, 10, 12 μm (in ascending order). All other conditions as in Fig. 2.

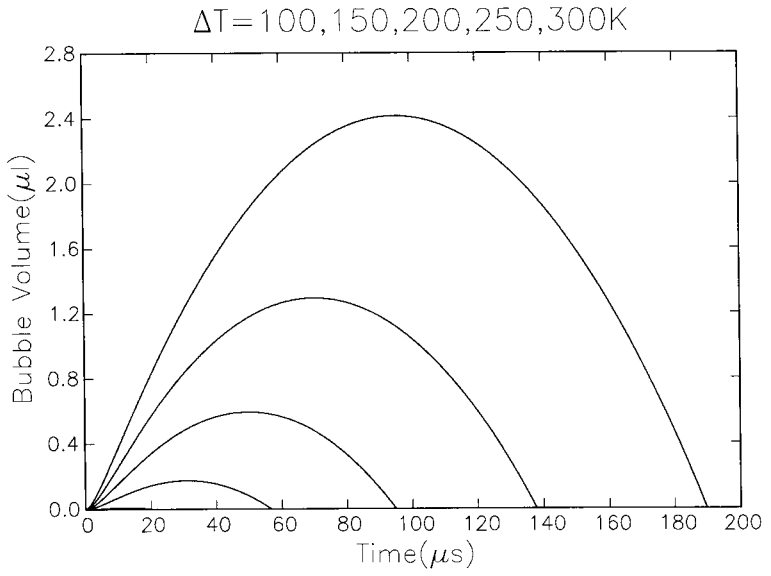

Fig. 10. Bubble volume vs time for different initial liquid superheats, $\Delta T = 100$, 150, 200, 250, 300 K (in ascending order). All other conditions as in Fig. 2.

in the left half of the figure are the temperature distributions along the bubble equator and into the solid, that occupies the region to the left of -50 μm, at the same times. The dotted lines are the temperature distributions at 90 μs during the collapse. In this figure all the lines begin at the instantaneous position of the bubble surface. The dotted line corresponding to 90 μs shows that the liquid around the bubble is very little heated near the end of the collapse. One must deduce that most of the initial thermal energy is conducted into the wall, as this figure also suggests.

We can now contrast the basic features just described with the effect of introducing changes in the various parameters of the problem.

We first look at the effect of the initial bubble size, other conditions being the same as before. Fig. 8

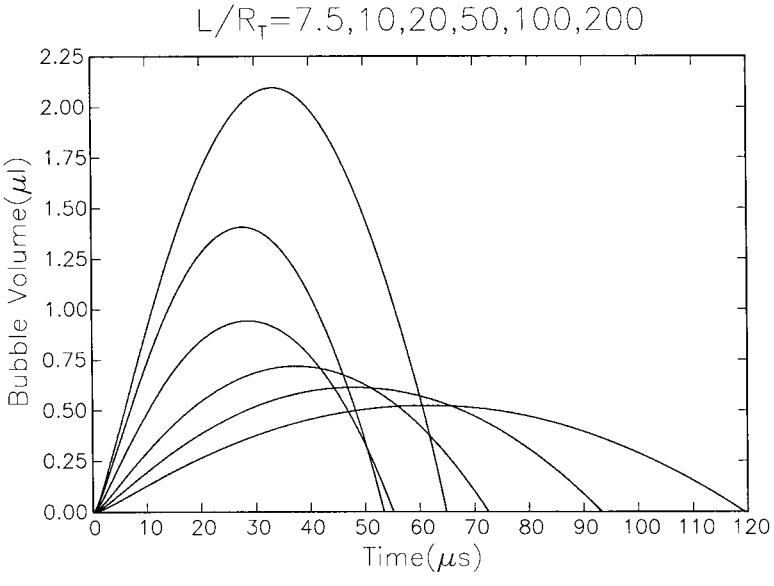

Fig. 11. Bubble volume vs time for different channel aspect ratios $L/R_T = 7.5$, 10, 20, 50, 100, 200 (in descending order). In all cases, the bubble is at the center of the channel. All other conditions as in Fig. 2.

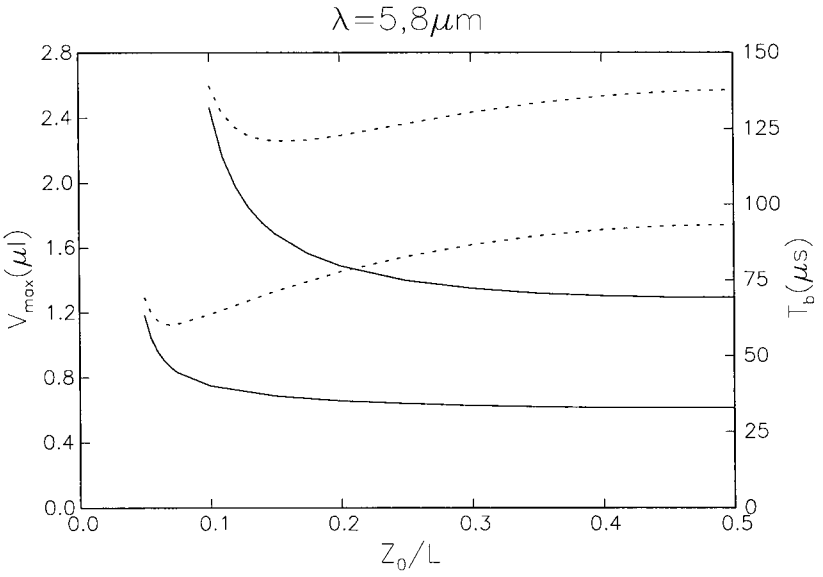

Fig. 12. Maximum bubble volume (left scale, solid lines) and lifetime (right scale, dotted lines) versus position of the bubble center in the channel. The lower pair of curves is for the temperature distribution Eq. (26) with $\lambda = 5$ μm, and the upper one for $\lambda = 8$ μm. The channel aspect ratio is $L/R_T = 100$. All other conditions as in Fig. 2.

shows the effect of changing the initial bubble size adjusting λ so as to maintain the same total amount of initial energy in the liquid:

$$\int_{a(0)}^{\infty} \Delta T \exp\left[-\frac{r - a(0)}{\lambda} \right] r^2 \, dr = \text{const.} \tag{37}$$

This constraint has the effect of making the heated layer near a bigger bubble thinner. As $a(0)$ increases from 0.2 to 5 μm, there is a major increase in the maximum volume and lifetime of the bubble. The result clearly indicates that there is a big gain in efficiency concentrating the heating in the vicinity of the bubble surface, so that more heat can be used to evaporate the liquid rather than being conducted away. In practice this can be achieved by sizing and shaping the heater in such a way that the liquid pre-heating can be made as short as possible, compatibly with the final desired volume of the bubble.

For a given $a(0) = 5$ μm, Fig. 9 illustrates the effect of the heated layer thickness $\lambda = 4$, 6, 8, 10, 12 μm, with ΔT fixed at 250 K. As the layer thickness is increased which, in practice, means a longer pre-heating, the total amount of thermal energy available also increases, the bubble grows bigger, and lasts longer. The bubble behavior is also very sensitive to the value of ΔT, as Fig. 10 shows.

For a bubble in the center of the tube, the tube length determines the mass of the liquid slugs that need to be pushed outward during the growth process and therefore has a strong effect on the bubble lifetime. Fig. 11 shows that, for a given initial thermal energy, the effect is not monotonic, however. When the tube length is small (e.g. $L = 0.75$ mm, $L/R_T = 15$), the bubble readily expels the liquid, the loading on its ends becomes small, and the potential to induce collapse less. As a consequence, the volume and the lifetime of the bubble are both large. As the tube is made longer, inertia increases, which causes a decrease of the maximum volume, but also a lengthening of the bubble life. For the conditions of this example, the minimum lifetime is of about 53 μs and is attained for L/R_T between 10 and 20.

Finally, we show in Fig. 12 graphs of the bubble lifetime and maximum volume as they depend on the initial position of the bubble for $L/R_T = 100$ and two different values of λ, 5 and 8 μm. In both cases, when the bubble is generated very close to one of the tube ends, both its lifetime and volume increase for the same reason as mentioned before in connection with Fig. 11. As the bubble is moved toward the middle of the tube, the lifetime decreases and then increases again. The minimum moves toward the open end as the energy decreases. The bubble volume is instead monotonic and is a minimum when the mass loading is maximum, i.e. when the bubble is in the middle of the tube.

5. Conclusions

In this paper we have studied the thermo-fluid

dynamics of the growth and collapse of a vapor bubble in a small channel connecting two liquid reservoirs.

In spite of several simplifications, the model exhibits the correct qualitative trends and helps one understand what are the controlling physical processes. While the initial impulse to the bubble growth comes from a strong localized superheat, already after about 10% of the bubble lifetime the internal pressure has become negligible and the dynamics of the bubble is governed mostly by inertia. The maximum volume of the bubble is found to be very sensitive to the amount of energy available for its growth measured both in terms of liquid superheat and thickness of the heated layer. The implication is that in order to grow a sizeable bubble one should either use a relatively large heater or add thermal energy to the liquid at a slow rate, at least initially. The channel wall plays an important role as a sink of energy, which is desirable if the objective is to grow and collapse many bubbles in sequence without causing a significant accumulated heating of the system. The length of the channel and the position of the bubble in it are also important factors determining the lifetime and maximum volume of the bubble. This fact implies that an equal heating will produce different bubbles at different positions along the channel.

Acknowledgement

This study has been supported by AFOSR under grant F49620-96-1-0386.

References

[1] T.K. Jun, C.J. Kim Microscale pumping with traversing bubbles in microchannels, in: Solid-State Sensor and Actuator Workshop, pp. 144–147, Hilton Head Island, June 1996. Transducer Research Foundation. 96TRF-0001 1996.

[2] P. Gravesen, J. Branebjerg, O.S. Jensen, Microfluidics—A review, J. Micromech. Microeng. 3 (1993) 168–182.

[3] T.S.J. Lammerink, M. Elwenspoek, J.H.J. Fluitman, Integrated micro-liquid dosing system, in: Micro Electromechanical Systems, I.E.E.E., 1993, pp. 254–259.

[4] R. Miyake, T.S.J. Lammerink, M. Elwenspoek, J.H.J. Fluitman, Micromixer with fast diffusion, in: Micro Electromechanical Systems, I.E.E.E., 1993, pp. 248–253.

[5] A. Olson, O. Larsson, J. Holm, L. Lundbladh, O. Öman, G. Stemme, Valve-less diffuser micropump fabricated using thermoplastic replication, Sensors and Actuators A64 (1998) 63–68.

[6] X.F. Peng, H.Y. Hu, B.X. Wang, Boiling nucleation during liquid flow in microchannels, Int. J. Heat Mass Transfer 41 (1998) 101–106.

[7] X.F. Peng, B.X. Wang, Liquid flow and heat transfer in microchannels with/without phase change, in: G. Hewitt (Ed.), Proceedings of the 10th International Heat Transfer Conference, Ind. Eng. Chem., 1994, pp. 159–177.

[8] P.A. Kew, K. Cornwell, Confined bubble flow and boiling in narrow spaces, in: G. Hewitt (Ed.), Proceedings of the Xth International Heat Transfer Conference, I. Eng. Chem., 1994, pp. 473–478.

[9] S. Kakac, B. Kilkis, F.A. Kulacki, F. Arinc (Eds.), Convective Heat and Mass Transfer in Porous Media, NATO ASI, Vol. 196, Kluwer, Dordrecht, 1991.

[10] C. Satik, Y.C. Yortsos, A pore-network study of bubble growth in porous media driven by heat transfer, J. Heat Transfer 118 (1996) 455–462.

[11] L.W. Swanson, G.P. Peterson, The interfacial thermodynamics of micro heat pipes, J. Heat Transfer 117 (1995) 195–201.

[12] D. Khrustalev, A. Faghri, Thick-film phenomenon in high-heat-flux evaporation from cylindrical pores, J. Heat Transfer 119 (1997) 272–278.

[13] A. Asai, T. Hara, I. Endo, One-dimensional model of bubble growth and liquid flow in bubble jet printers, Jap. J. Appl. Phys. 26 (1987) 1794–1801.

[14] A. Asai, Bubble dynamics in boiling under high heat flux pulse heating, J. Heat Transfer 113 (1991) 973–979.

[15] L. Lin, A.P. Pisano, Bubble forming on a micro line heater, in: D. Cho (Ed.), Micromechanical Sensors, Actuators, and Systems, A.S.M.E., DSC—Vol. 32, 1991, pp. 147–163.

[16] L. Lin, A.P. Pisano, V.P. Carey, Thermal bubble formation on polysilicon resistors, J. Heat Transfer 120 (1998) 735–742.

[17] H. Yuan, A. Prosperetti Thermo-fluid mechanic model for a bubble-actuated pump. In preparation.

[18] H.N. Oğuz, A. Prosperetti, The natural frequency of oscillation of gas bubbles in tubes, J. Acoust. Soc. Am. 103 (1998) 3301–3308.

[19] H.N. Oğuz, J. Zeng, Boundary integral simulations of bubble growth and detachment in a tube, in: Boundary Elements XVII, Computational Mechanics Publications, Madison, WI, 1995.

[20] H.N. Oğuz, J. Zeng, Axisymmetric and three-dimensional boundary integral simulations of bubble growth from an underwater orifice, Engineering Analysis with Boundary Elements 19 (1995) 313–330.

[21] X.M. Chen, A. Prosperetti, Thermal processes in the oscillations of gas bubbles in tubes, J. Acoust. Soc. Am. 104 (1998) 1389–1398.

[22] L.D. Landau, E.M. Lifshitz, Statistical Physics, Pergamon, 1959.

[23] L.D. Landau, E.M. Lifshitz, Fluid Mechanics, Pergamon, 1959.